2023 IEEE International Conference on Robotics and Automation (ICRA 2023)
May 29 - June 2, 2023. London, UK

Discrete-time model based control of soft manipulator with FBG sensing

Enrico Franco[1], Ayhan Aktas[1], Shen Treratanakulchai[1,2], Arnau Garriga-Casanovas[1], Abdulhamit Donder[3], and Ferdinando Rodriguez y Baena[1]

***Abstract*— In this article we investigate the discrete-time model based control of a planar soft continuum manipulator with proprioceptive sensing provided by fiber Bragg gratings. A control algorithm is designed with a discrete-time energy shaping approach which is extended to account for control-related lag of digital nature. A discrete-time nonlinear observer is employed to estimate the uncertain bending stiffness of the manipulator and to compensate constant matched disturbances. Simulations and experiments demonstrate the effectiveness of the controller compared to a continuous time implementation.**

I. Introduction

Model-based control of soft manipulators poses considerable technical challenges, since these systems possess more degrees-of-freedom (DOFs) than actuators and sensors. As a result, the use of classical model-based control methods is either precluded or it requires neglecting the dynamics of the unactuated DOFs, which can compromise performance in some cases. Conversely, energy shaping controllers [1] can account for underactuation thus yielding more consistent performance compared to classical approaches. The use of proprioceptive sensing holds promise to facilitate the controller design, since it could enable full-state feedback, as opposed to output feedback. In this respect, promising sensing modalities include piezoresistive sensing skins [2], [3], and fiber optic solutions [4], [5]. Among the latter, fiber Bragg grating (FBG) has been shown to provide acceptable accuracy and small footprint [5], [6]. Regardless of the sensing principle, many proprioceptive sensing solutions involve reconstructing the position or the shape of the soft manipulator from multiple measurements by employing digital signal processing or data driven techniques. As a result, the computation of the control input can be affected by lag, which should be taken into account in the controller design to avoid performance degradation. In principle, a control-related lag bears some similarity to the effect of actuator dynamics, which has been investigated in recent works [7], [8], [9]. Nevertheless, control-related lag is digital in nature hence a discrete-time control formulation is more appropriate to account for its effect [10], [11]. A further challenge is the effect of proprioceptive sensors on the mechanical properties of the soft manipulators, which may result in uncertain model parameters. While recent controllers for soft robots have included either nonlinear observers [12], [1] or integral actions [13] to account for external disturbances, the study of model uncertainties has received less attention.

In this paper we investigate the model based control of a planar soft continuum manipulator with proprioceptive FBG sensing by employing a discrete-time port-Hamiltonian formulation and an energy shaping control approach. The main contributions of this work include the following points.

- A new discrete-time controller design is presented, that extends the energy shaping formulation [14], [10] by accounting for control-related lag of digital nature.
- A discrete-time nonlinear observer is constructed to estimate the uncertain bending stiffness of the manipulator and to compensate for constant matched disturbances.
- Stability conditions are discussed, and numerical simulations and experiments are employed to assess the performance of the proposed controller compared a model-based continuous time implementation [1].

Section II presents the system model, and Section III details the controller design. Section IV presents simulations and experimental results, and Section V concludes the paper.

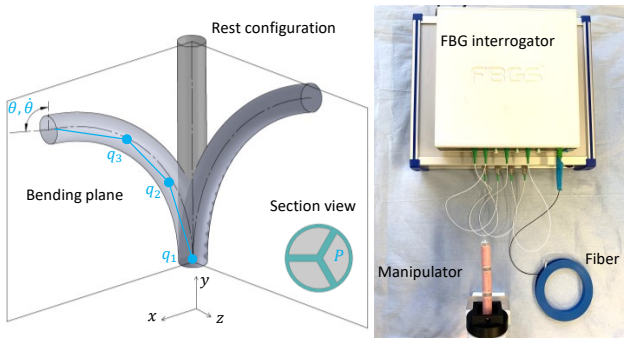

Fig. 1. Schematic of soft continuum manipulator and test setup.

II. System model

We consider a soft continuum manipulator such as [15], which has three internal chambers and an inextensible central axis to prevent elongation. While the manipulator can bend on any plane by pressurizing multiple chambers simultaneously, we assume for simplicity but without loss of generality

This research was supported by the Engineering and Physical Sciences Research Council (grant number EP/W004224/1) and partially by a collaboration with the Multi-Scale Medical Robotics Centre, The Chinese University of Hong Kong. The work of Ayhan Aktas and Abdulhamit Donder was supported by the Republic of Turkey.

[1]Mechatronics in Medicine Laboratory, Mechanical Engineering Department, Imperial College London, London, SW7 2AZ UK.
[2]Biomedical and Robotics Technology Laboratory, Mahidol University, Nakon Pathom, Thailand.
[3]Boston Children's Hospital, Harvard Medical School, USA.
Corresponding author: Enrico Franco, ef1311@imperial.ac.uk

that a single pressure source supplies only one chamber. In the absence of lag, the control input corresponds to the bending moment y generated by the pressure P set by a digital regulator. Due to the fast response of the regulator ($\leq$ 10 ms) compared to the that of the manipulator [13], the pressure dynamics is not accounted for explicitly in this work. At equilibrium and in the absence of external forces, the tip rotation θ of the manipulator depends on the bending moment y due to the pressure P, according to

$$\theta = y/k^{'}, \tag{1}$$

where $k^{'}$ is the bending stiffness [16].

The dynamics of the soft continuum manipulator on the bending plane is approximated with a rigid-link model that has n virtual elastic pin joints of stiffness k and damping D_0 in series [17] (see Figure 1). This approach is based on the *pseudo-rigid-body model* which approximates the force/deflection relationship of a flexible mechanism by introducing virtual elastic joints [18]. Indicating with q_i the angle of link i relative to link $i-1$ yields $\theta = \sum_{i=1}^{n} q_i$ and $k = nk^{'}$. In this case, the virtual joints q_i correspond to the FBG sensing elements, thus the resulting model has n DOFs and one control input, which acts equally on all joints. The mechanical energy of the system is $H(q,p) = \frac{1}{2}p^T M^{-1} p + \Omega$, where $M = M^T > 0$ is the inertia matrix, $p = M\dot{q}$ is the momenta, and $\Omega = \frac{1}{2}kq^T q$ is the potential energy [13]. Employing the Euler approximation, the discrete-time open-loop dynamics in port-Hamiltonian form in the presence of matched disturbances δ is

$$\begin{bmatrix} q^+ \\ p^+ \end{bmatrix} = \begin{bmatrix} q \\ p \end{bmatrix} + T \begin{bmatrix} 0 & I^n \\ -I^n & -D \end{bmatrix} \begin{bmatrix} \nabla_q H \\ \nabla_p H \end{bmatrix} + T \begin{bmatrix} 0 \\ G \end{bmatrix} (y - \delta) \tag{2}$$

where q^+ and p^+ are the updated values of the states, $T > 0$ is the sampling interval, I is the identity matrix, $D = D_0 I > 0$ is the physical damping matrix, $\nabla_q H$ and $\nabla_p H$ represent the continuous gradients in q and p. Since the pressure affects all joints in the same way, the input matrix is $G^T = [1\ 1\ 1]$ for $n = 3$. In this work, the bending moment y generated by the pressure P is related to the control input u according to the first-order dynamics in discrete-time

$$y^+ = y(1 - \epsilon T) + h_0 \epsilon T u, \tag{3}$$

where $0 < \epsilon < 1/T$ is a parameter characterizing the lag (i.e., smaller ϵ for larger lag) and $h_0 > 0$ is a constant depending on the units of measurement of the pressure. Using the Euler approximation, which is not Hamiltonian preserving, is appropriate in the context of energy shaping control [10], [19], since the latter does not aim to preserve the Hamiltonian H but to reshape it into H_d. For the purpose of generality, lag is described by (3) without going into the detail of the specific signal processing techniques employed for FBG sensing. This approach allows to account also for hardware-related lag, considering that the response of some actuators (i.e., of the digital pressure regulator in this case) can be approximated with a first-order model. The following assumptions are introduced for control purposes.

Assumption 1. The bending stiffness $k > 0$ is uncertain but bounded; ϵ and all other model parameters are known.

Assumption 2. The position q and the velocity $\dot{q}$ are measurable and bounded, that is $0 \leq q \leq \sigma_0$ and $|\dot{q}| \leq \sigma_1$. The bending moment y is known from (3) and bounded, that is $0 \leq y \leq \sigma_2$. The positive bounds $\sigma_0, \sigma_1, \sigma_2$ are known.

Assumption 3. The manipulator moves on an horizontal plane hence Ω does not account for gravity effects. The matched disturbances δ are unknown but constant.

III. Controller design

The control goal is the regulation of the tip rotation to $\theta = \theta^* > 0$ in the presence of an uncertain stiffness k, an unknown δ, and of a known lag defined by ϵ. Accounting for δ is motivated by the fact that no bending is observed in our prototype until the pressure is larger than a given threshold.

A. Discrete-time observer

The stiffness k and the disturbance δ are estimated with a nonlinear observer constructed according to the *Immersion and Invariance* methodology [20] in its discrete implementation [21]. The estimation errors ζ_0 and ζ_1 are defined as

$$\begin{aligned} \zeta_0 &= \widehat{\delta} + p^T \beta_0^- - \delta, \\ \zeta_1 &= \widehat{k} + p^T \beta_1^- - k, \end{aligned} \tag{4}$$

where the stiffness estimate is $\tilde{k} = \widehat{k} + p^T \beta_1^-$ and the disturbance estimate is $\tilde{\delta} = \widehat{\delta} + p^T \beta_0^-$. The update laws for the functions β_0^-, β_1^- and the states $\widehat{\delta}$ and $\widehat{k}$ are given by

$$\begin{aligned} \widehat{\delta}^+ &= \widehat{\delta} - T\alpha G^T \nabla_q \left(\frac{1}{2} p^T M^{-1} p \right) \\ &- T\alpha G^T \left(\left(\widehat{k} - \alpha p^T q^- \right) q + D\nabla_p H - G(y - \widehat{\delta} + \alpha p^T G) \right), \\ \widehat{k}^+ &= \widehat{k} + \alpha p^T (q - q^-) - T\alpha q^T \nabla_q \left(\frac{1}{2} p^T M^{-1} p \right) \\ &- T\alpha q^T \left(\left(\widehat{k} - \alpha p^T q^- \right) q + D\nabla_p H - G(y - \widehat{\delta} + \alpha p^T G) \right), \\ \beta_0^- &= -\alpha G,\ \beta_1^- = -\alpha q^- \end{aligned} \tag{5}$$

with α a constant tuning parameter and q^- indicating the position of the virtual joints at the previous sampling interval.

Proposition 1: Consider system (2) with *Assumptions 1* to *3* and with the observer defined by the update laws (5). Then $\overline{\zeta} = G\zeta_0 + q\zeta_1$ is bounded and converges to zero for $\alpha > 0$.

Proof: Computing (4) at the next time step and substituting (2) yields

$$\begin{aligned} \zeta_0^+ &= \widehat{\delta}^+ + p^T \beta_0 + T\beta_0^T \left(-\nabla_q \left(\frac{1}{2} p^T M^{-1} p \right) \right) \\ &+ T\beta_0^T \left(- \left(\widehat{k} + p^T \beta_1^- - \zeta_1 \right) q - D\nabla_p H \right) \\ &+ T\beta_0^T G \left(y - \widehat{\delta} - p^T \beta_0^- + \zeta_0 \right) - \delta, \\ \zeta_1^+ &= \widehat{k}^+ + p^T \beta_1 + T\beta_1^T \left(-\nabla_q \left(\frac{1}{2} p^T M^{-1} p \right) \right) \\ &+ T\beta_1^T \left(- \left(\widehat{k} + p^T \beta_1^- - \zeta_1 \right) q - D\nabla_p H \right) \\ &+ T\beta_1^T G \left(y - \widehat{\delta} - p^T \beta_0^- + \zeta_0 \right) - k. \end{aligned} \tag{6}$$

Substituting (5) into (6) yields

$$\zeta_0^+ = \zeta_0\left(1 - T\alpha G^T G\right) - \zeta_1 \alpha T G^T q^-,$$
$$\zeta_1^+ = \zeta_1\left(1 - T\alpha q^T q^-\right) - \zeta_0 \alpha T G^T q^-.$$

Defining the storage function $W = \zeta_0^2 + \zeta_1^2$ and computing its increment over a time step while employing the Mean Value Theorem yields after factoring common terms

$$W^+ - W = -\alpha T \left(G\zeta_0 + q\zeta_1\right)^T \left(G\zeta_0 + q\zeta_1\right) + \mathcal{O}(T^3). \tag{7}$$

Thus $W^+ - W < 0$ for $\alpha > 0$ and for a sufficiently small T. It follows from (7) and from *Assumption 2* that $\overline{\zeta} = G\zeta_0 + q\zeta_1 \in \mathcal{L}^2 \cap \mathcal{L}^\infty$. Computing $\dot{\zeta}_0, \dot{\zeta}_1$ from ζ_0^+, ζ_1^+ at $T \to 0$, yields $\dot{\overline{\zeta}} \in \mathcal{L}^\infty$, hence $\overline{\zeta}$ is bounded and converges to zero asymptotically [22] □

Remark 1. Differently from our prior works [8], [1], the observer (5) requires full state feedback and results in stronger convergence properties. Computing (7) at $q^- = 0$ without employing the Mean Value Theorem yields $W^+ - W = \zeta_0^2\left(\left(1 - T\alpha G^T G\right)^2 - 1\right)$, which is verified for all $0 < \alpha < \frac{2}{Tn}$, where $G^T G = n$. The upper limit on α decreases with the sampling interval T and with n, thus a slower sampling and more FBG sets require a less aggressive tuning of the observer (5), which is in agreement with engineering practice. Note finally that setting $q^- = 0$ results in $\zeta_1^+ = \zeta_1$, which however is a limit conditions, since $y > 0$ yields $\theta > 0$ from (1), while $\theta^* > 0$.

B. Discrete-time energy shaping control

Before detailing the controller design we recall the following result from [10] for completeness.

Theorem 3.2 [10]: Consider the Euler model (2) with control input y, Hamiltonian H, and the discrete-time controller

$$\begin{aligned} y &= \overline{u}_e + u_d \\ \overline{u}_e &= G^\dagger\left(\nabla_q H - M_d M^{-1}\left(\overline{\nabla_q H_d}\right) + J_2 M_d^{-1} p\right), \\ u_d &= -K_v G^T M_d^{-1} p, \end{aligned} \tag{8}$$

where $G^\dagger = \left(G^T G\right)^{-1} G^T$ and $J_2 = -J_2^T$ is a free matrix. The closed-loop Hamiltonian is $H_d = \frac{1}{2} p^T M_d^{-1} p + \Omega_d$ and $\overline{\nabla_q H_d} = \nabla_q H_d + T\kappa L_V^{'} M^{-1} p$, with $L_V^{'}$ defined so that $P = \left(M_d^{-1} G G^\dagger M_d M^{-1} L_V^{'} M^{-1}\right) \geq 0$, and $\kappa, K_v > 0$ are tuning parameters. The parameters M_d and Ω_d are such that

$$G^\perp\left(\nabla_q H - M_d M^{-1} \nabla_q H_d + J_2 \nabla_p H_d\right) = 0, \tag{9}$$

where $G^\perp$ is such that $G^\perp G = 0$ and $\text{rank}(G) + \text{rank}(G^\perp) = n$. Then, the equilibrium $(q, p) = (q^*, 0)$, with $q^* = \text{argmin}(\Omega_d)$ is semi-globally practically asymptotically stable (SPAS) for sufficiently small sampling intervals [23] provided that the output $G^T M_d^{-1} p$ is detectable □

The control law u for system (2-3) is designed following a similar procedure to [9], which is modified here to account for the control-related lag. Thus, the closed-loop dynamics in port-Hamiltonian form becomes

$$\begin{bmatrix} q^+ \\ p^+ \\ y^+ \end{bmatrix} = \begin{bmatrix} q \\ p \\ y \end{bmatrix} + T \begin{bmatrix} 0 & S_{12} & S_{13} \\ -S_{12}^T & -S_{22} & S_{23} \\ -S_{13}^T & -S_{23}^T & -S_{33} \end{bmatrix} \begin{bmatrix} \overline{\nabla_q H_d} \\ \nabla_p H_d \\ \nabla_P H_d \end{bmatrix} + \eta, \tag{10}$$

where $\eta^T = T[0\ \overline{\zeta}\ 0]$ accounts for the estimation error $\overline{\zeta}$, $H_d = \Omega_d + \frac{1}{2k_m} p^T M^{-1} p + \frac{1}{2}\varsigma^2$ is a positive definite storage function, and $\overline{\nabla_q H_d} = \nabla_q H_d + T\kappa L_V G G^T M^{-1} p$ where $L_V > 0$ is a scalar. The potential energy is defined as in [8], [13] such that it satisfies the minimizer condition $\theta^* = \text{argmin}\,(\Omega_d)$ and the matching condition (9), that is $\Omega_d = \frac{\widehat{k}}{2k_m}\left(\sum_{i=1}^n q_i^2 + \frac{k_p}{\widehat{k}}\left(\theta - \theta^*\right)^2 - \frac{\theta^2}{n}\right)$ with $M_d = k_m M, J_2 = 0$, and the tuning parameters $k_p > 0$ and $k_m > 0$. The term ς in H_d is defined as

$$\varsigma = y - \frac{\widehat{k}}{n}\theta + k_p(\theta - \theta^*) - \widehat{\delta} + L_V \kappa T k_m \dot{\theta}. \tag{11}$$

Since (11) contains the observer states $\widehat{k}, \widehat{\delta}$, the error $\overline{\zeta}$ is included in (10). The terms S_{ij} in (10) are defined as

$$\begin{aligned} S_{12} = k_m,\ S_{13} = -k_m \nabla_p \varsigma, \\ S_{22} = k_m(D - \alpha(GG^T + q^- q^T)M),\ S_{33} = k_i, \\ S_{23} = G\left(1 + G^\dagger k_m \nabla_q \varsigma + G^\dagger S_{22} \nabla_p \varsigma\right) \\ + G^{\perp^T}\left(G^\otimes k_m \nabla_q \varsigma + G^\otimes S_{22} \nabla_p \varsigma\right), \end{aligned} \tag{12}$$

where k_i is a tuning parameter and $G^\otimes = (G^\perp G^{\perp^T})^{-1} G^\perp$. The control input written in compact form is

$$u = \frac{y}{h_0} - \frac{1}{\epsilon h_0}\left(S_{13}^T \overline{\nabla_q H_d} + S_{23}^T \nabla_p H_d + S_{33}\varsigma\right) \tag{13}$$

where S_{13}, S_{23}, S_{33} are given in (12).

Proposition 2: Consider system (2-3) with *Assumptions 1* to *3* in closed-loop with the control law (13) and the observer defined by the update laws (5). Define the positive constant parameters k_i, k_m, α, L_V, and κ such that

$$\Theta = \begin{bmatrix} D_d & k_m DB & \frac{I}{2} \\ k_m DB^T & k_i + k_m DB^T B & \frac{1}{2}B \\ \frac{I}{2} & \frac{1}{2}B^T & \alpha \end{bmatrix}, \tag{14}$$

is positive definite, where $D_d = S_{22} + GG^T \kappa T L_V k_m^2$ and $B = T\kappa L_V k_m M^{-1} G$. Then the equilibrium $\theta = \theta^*$ is SPAS for sufficiently small sampling intervals T. Simplified conditions for $\Theta > 0$ corresponding to an infinitesimal T are

$$k_i > 0,\ 4k_m(D_0 I - \alpha(GG^T + q^- q^T)M)\alpha > 1. \tag{15}$$

Proof: Note first that substituting the control law (13) into (2) and (3) yields (10) with the parameters (12). In particular, equating (2-3) and (10) yields the matching equations

$$M^{-1} p = S_{12} M_d^{-1} p + S_{12}\varsigma \nabla_p \varsigma + S_{13}\varsigma \nabla_y \varsigma, \tag{16}$$

$$\begin{aligned} G(y - \delta) - \nabla_q H - D\nabla_p H = \\ \overline{\zeta} - S_{22}\left(M_d^{-1} p + \varsigma \nabla_p \varsigma\right) + S_{23}\varsigma \nabla_y \varsigma \\ -S_{12}^T\left(\nabla_q H_d + T\kappa L_V^{'} M^{-1} p + \varsigma \nabla_q \varsigma\right), \end{aligned} \tag{17}$$

$$
\begin{aligned}
y(1-\epsilon T)+h_0\epsilon T u = y - TS_{33}\varsigma\nabla_y\varsigma \\
-TS_{23}^T\left(M_d^{-1}p+\varsigma\nabla_p\varsigma\right) \\
-TS_{13}^T\left(\nabla_q H_d + T\kappa L_V^{'}M^{-1}p+\varsigma\nabla_q\varsigma\right),
\end{aligned} \tag{18}
$$

where it follows form (11) that $\nabla_y\varsigma = 1$, while $L_V^{'} = L_V GG^T$. In particular, (16) is verified by $M_d = k_m M$ and S_{12}, S_{13} given in (12). Pre-multiplying each side of (17) by $G^{\perp}$ while substituting (11) and (12) yields (9) which is satisfied by design with $J_2 = 0$ and Ω_d as previously defined. Instead, pre-multiplying (17) by $G^{\dagger}$ yields $\varsigma = -G^{\dagger}k_m\varsigma\nabla_q\varsigma - G^{\dagger}S_{22}\varsigma\nabla_p\varsigma + G^{\dagger}S_{23}\varsigma$, which is verified by S_{22}, S_{23} given in (12). Finally, (13) verifies (18).

Before proving the stability claim, we proceed by showing that the structure chosen for the matrix $L_V^{'}$, that is $L_V^{'} = L_V GG^T$, satisfies the condition of *Theorem 3.2* [10]. Computing $P = \left(M_d^{-1}GG^{\dagger}M_d M^{-1}L_V^{'}M^{-1}\right) \geq 0$ with $M_d = k_m M$, substituting $L_V^{'}$, and refactoring terms yields

$$
\begin{aligned}
P &= M^{-1}GG^{\dagger}MM^{-1}L_V GG^T M^{-1} \\
&= L_V M^{-1}GG^T M^{-1} \geq 0,
\end{aligned} \tag{19}
$$

which is verified by all $L_V > 0$ since $M = M^T > 0$, and $GG^T = \left(GG^T\right)^T \geq 0$ has all elements equal to one.

To prove the stability claim we define the Lyapunov function $\Psi = H_d + W$. Computing its increment over a time step along the trajectories of the closed-loop system (10) and using the Mean Value Theorem, while substituting (7) from *Proposition 1*, yields for a sufficiently small T

$$
\begin{aligned}
\Psi^+ - \Psi = -T\nabla_p H_d^T S_{22}\nabla_p H_d - Tk_i\varsigma^2 \\
-\alpha T\overline{\zeta}^T\overline{\zeta} - \kappa L_V T^2\nabla_p H_d^T GG^T M^{-1}p + T\nabla_p H_d^T\overline{\zeta} \\
+T(T\kappa L_V k_m)^2\varsigma G^T M^{-1}GG^T M^{-1}p + \mathcal{O}(T^3).
\end{aligned} \tag{20}
$$

Refactoring common terms in (20) yields

$$
\Psi^+ - \Psi = -Tz^T\Theta z + \mathcal{O}(T^3), \tag{21}
$$

where $z^T = \begin{bmatrix} M_d^{-1}p & \varsigma & \overline{\zeta} \end{bmatrix}$ while Θ is given in (14). If $\Theta > 0$ then $\Psi^+ - \Psi \leq 0$ and the equilibrium is stable. In case of infinitesimal T the inequalities (15) ensure that $\Theta > 0$. To conclude SPAS of the equilibrium, we use similar arguments to *Theorem 3.2* in [10]. To this end, note that $p, \varsigma \in \mathcal{L}^2 \cap \mathcal{L}^{\infty}$, $\overline{\zeta} \in \mathcal{L}^2$, and $\zeta_0, \zeta_1, q \in \mathcal{L}^{\infty}$. In addition, it follows from (10) computed at $T \to 0$ that $\dot{q}, \dot{p}, \dot{y} \in \mathcal{L}^{\infty}$ and from *Proposition 1* that $\dot{\overline{\zeta}} \in \mathcal{L}^{\infty}$ hence also $\dot{\varsigma} \in \mathcal{L}^{\infty}$. Thus $p, \varsigma, \overline{\zeta}$ and z are bounded and converge to zero asymptotically [22] for the continuous-time system corresponding to (10). Since $z = 0$ is the set of points where $\Psi^+ - \Psi = 0$, it implies $p^+ = p = 0, \varsigma = 0$, and $\overline{\zeta} = 0$. Computing p^+ from (10) at $z = 0$ yields $\nabla_q\Omega_d = 0$, while $\theta^* = \text{argmin}(\Omega_d)$ by design. Thus the equilibrium $\theta = \theta^*$ is the largest invariant set in $z = 0$ and it is asymptotically stable (see Corollary 3.1 in [24]). Therefore the equilibrium is SPAS for system (10), where the practical and semiglobal (in the parameter T) properties come from the fact that T is assumed sufficiently small [10]. Finally, computing (11) at $\dot{\theta} = \varsigma = 0$ and $\theta = \theta^*$ yields the bending moment at the equilibrium, that is $y^* = \frac{\tilde{k}}{n}\theta^* + \tilde{\delta}$ □

Remark 2. Differently from our previous work on soft continuum manipulators [13], the controller design includes a damping term dependent on the parameter L_V. As a result, the expressions of S_{23} in (12) and of the control law (13) are more complex. While the effect of the parameter L_V is similar to the damping assignment achieved in the IDA-PBC methodology [14] with the parameter K_v in (8), it originates instead from the discrete-time implementation. As a result, L_V does not affect the closed-loop damping represented by S_{22}. This implies that, while setting $K_v = 0$ as in [8], [9] preserves the physical damping D in closed loop, setting $L_V = 0$ in the discrete-time implementation effectively reduces the physical damping by a factor dependent on the sampling interval. To highlight this point, note that computing (17) while setting $L_V = 0$ in ς and $\alpha = 0$ requires redefining $S_{22} = k_m D - Tk_0 L_V GG^T \leq k_m D$. Note also that the parameter α is included in S_{22} giving raise to a so-called negative damping assignment. This is caused by the terms β_0 and β_1 in (5) and yields an upper limit on α in (15), which decreases with D. Thus, a smaller physical damping D requires a less aggressive tuning of the observer (5), which is in agreement with engineering practice. Verifying (15) ensures that $S_{22} > 0$ hence the detectabilty of the output $G^T\nabla_p H_d$, which is needed in *Theorem 3.2* [10], is not required in *Proposition 2*. This results in stronger stability properties, provided that physical damping $D > 0$ is present.

Remark 3. Assessing the condition $\Theta > 0$ requires solving an eigenvalue problem, which however can be done beforehand for each $0 \leq q \leq \sigma_0$, since (14) does not depend on either p or y. While the sampling interval T is included in (14), the parameter ϵ which characterizes the lag is not. This is because the control law (13) accounts explicitly for ϵ at the denominator. Thus a smaller value of ϵ in (3) corresponding to a longer lag amplifies the term in parenthesis in (13) and results in a larger control action. Neglecting the effect of control-related lag and assuming a sufficiently small sampling interval results in the continuous-time controller [1], which for the planar case is

$$
u = y = \frac{\tilde{k}}{n}\theta + K_p\left(\theta^* - \theta\right) - \frac{K_v}{K_m}\dot{\theta} + \tilde{\delta}, \tag{22}
$$

where K_p, K_m, K_v are tuning parameters, and K_v indicates damping assignment. The terms $\tilde{k}$ and $\tilde{\delta}$ are computed with (5), thus also (22) requires full state feedback.

IV. Results of simulations and experiments

A. Simulation results

Simulations have been conducted in MATLAB using an ODE23 solver and the initial conditions $(q, p, y, \widehat{k}, \widehat{\delta}) = (0, 0, 0, 1.5, 0)$. A sample-and-hold with sampling interval $T = 0.05$ seconds has been applied to the control input in order to simulate the effect of a digital controller. The model parameters are $n = 3, D_0 = 0.2, k = 4, h_0 = 1$ and the inertia matrix M is defined as in [13] with the parameters $l = 0.085, m = 0.01$. A constant disturbance $\delta = 1$ has also been included to account for the fact that the prototype does not bend until the pressure reaches a given threshold. The

tuning parameters for the control law (13) have been set as $k_p = 1, k_m = 2, k_i = 10, \alpha = 5, \kappa = 0.001, L_V = 0.001$, which ensure that $\Theta > 0$ in (14) and verify the inequalities (15). The values of k_p, k_m, k_i, α and their effect on performance are similar to our previous work [8]. Three different values of ϵ have been considered for illustrative purposes, that is $\epsilon = 1, \epsilon = 2, \epsilon = 5$ which correspond to a time constant of $\tau = 1, \tau = 0.5, \tau = 0.18$ respectively for a continuous-time first-order system. The tuning parameters for controller (22) have been set to $K_p = 1, K_m = 2$ for consistency, and $K_v = 0.4$ to obtain a similar response to controller (13) with $\epsilon = 5$. The observer (5) has been employed in both cases to compute $\widehat{k}$ and $\widehat{\delta}$ with $\alpha = 5$.

Figure 2 shows that the regulation goal $\theta = \theta^*$ is correctly achieved by controller (13) with a similar transient in all conditions, requiring a larger control input for smaller values of ϵ. The baseline controller (22) shows a less consistent response since it does not directly account for lag. In particular, selecting a suitable K_v for $\epsilon = 5$ yields a slower convergence in case of smaller ϵ (i.e., larger lag). While it is certainly possible to modify the tuning parameters of controller (22) for each operating condition, there is no explicit relationship between the values of K_p, K_m, K_v and ϵ. Consequently, finding suitable tuning parameters for (22) involves trial and error, which is a disadvantage in engineering practice.

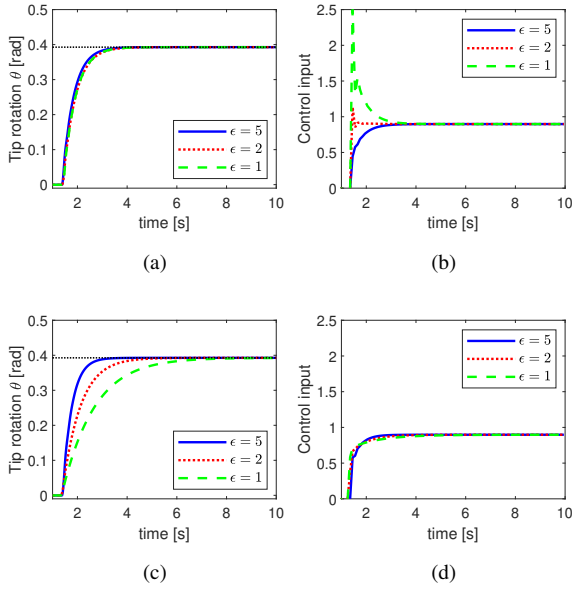

Fig. 2. Simulation results for system (2-3) comparing controller (13) with controller (22) for different parameters ϵ: (a) tip rotation θ with (13); (b) control input u with (13); (c) θ with (22); (d) u with (22).

B. Experimental results

The controllers (13) and (22) have been compared by performing experiments on a soft continuum manipulator prototype that measures 12 mm in diameter, 85 mm in length, and that has an approximate mass $m = 10$ grams (see Figure 1). The position q and the velocity $\dot{q}$ have been computed from an FBG sensor located in the central working

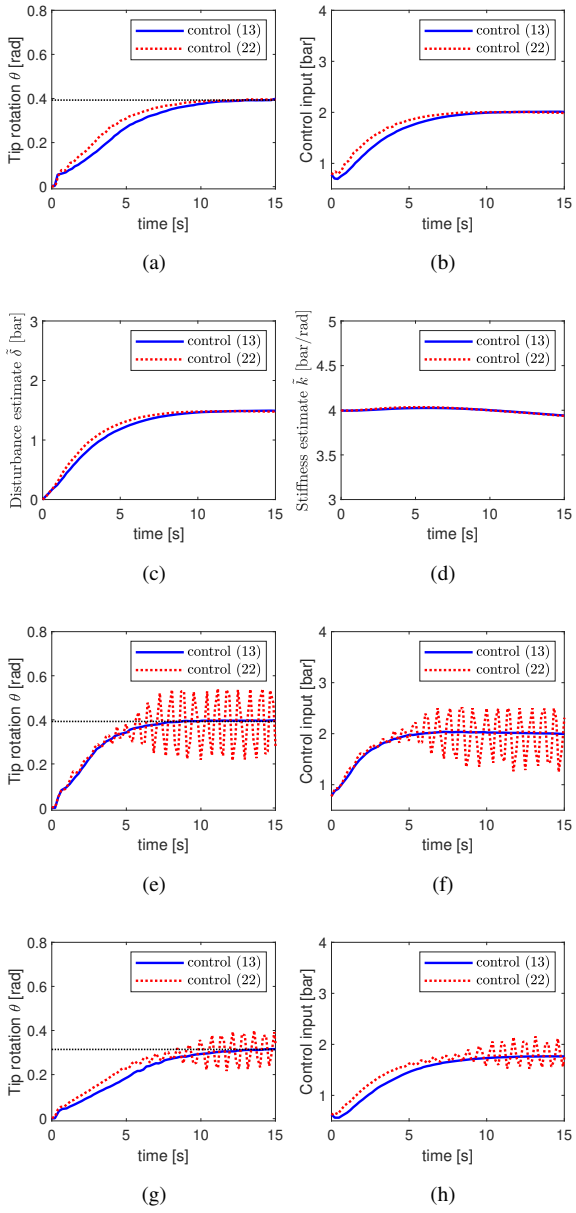

Fig. 3. Experimental results for system (2-3) comparing controller (13) with controller (22): (a) tip rotation θ with $\alpha = 2$ and $\theta^* = \pi/8$; (b) control input u; (c) disturbance estimate $\tilde{\delta}$; (d) stiffness estimate $\tilde{k}$; (e) θ with $\alpha = 5$ and $\theta^* = \pi/8$; (f) control input u; (g) θ with $\alpha = 2$ and $\theta^* = \pi/10$; (h) control input u.

channel of the manipulator. We have employed an FBG-inscribed multi-core fiber with $n = 3$ FBG sets, each 5mm long, corresponding to the virtual joints of the rigid-link model. The angles of the virtual joints have been computed with a piecewise constant curvature reconstruction method (see [6] for details). A Matlab script has been employed to acquire data from the FBG interrogator (FBGS International NV, Geel, Belgium) and to provide the control signal to a digital pressure regulator (Tecno Basic, Hoerbiger, Germany) that supplies one chamber of the manipulator along the whole length. The script communicates with the pressure

regulator through a microcontroller (mbed NXP LPC1768, NXP Semiconductors) via serial link (baud rate 921600). The sampling frequency of the FBG interrogator is 20 Hz (corresponding to $T = 0.05$ seconds in the simulations), and the same values of the model parameters and of the tuning parameters have been used as in the simulations. The bending stiffness of the prototype is uncertain, thus we have initialized the observer states in (5) as $\widehat{k} = 4$ bar/rad and $\widehat{\delta} = 0$ bar. The control-related lag is described by $\epsilon = 5$, corresponding to a time constant $\tau = 0.18$, which accounts for signal processing of the FBG measurements and for the response of the digital pressure regulator.

Figure 3a, 3b, 3c and 3d show that both controllers yield similar transients, control input, and adaptive estimates $\widehat{k}$ and $\widehat{\delta}$ with equal tuning parameters (i.e., $\alpha = 2, k_p = K_p = 1$) and $\theta^* = \pi/8$. Instead, Figure 3e shows that employing $\alpha = 5$ yields a faster response with controller (13) (i.e., settling time ≈ 7 seconds) but results in oscillations with controller (22) even though the same tuning is used in both cases. Similarly, Figure 3g shows that employing the same tuning parameters as Figure 3a (i.e., $\alpha = 2, k_p = K_p = 1$) but a different set-point (i.e., $\theta^* = \pi/10$), controller (13) preserves a similar transient (i.e., settling time ≈ 12 seconds), while controller (22) gives an oscillatory response. In summary, controller (13) yields a more consistent performance across different operating conditions since it explicitly accounts for the control-related lag. The slower response of the controllers in the experiments compared to the simulations is due to the higher damping and higher pressure threshold of the prototype (i.e., $\tilde{\delta} > 1$ bar in Figure 3c). A video of the experiments has been provided as a supplementary file.

V. Conclusion

In this work we have investigated the model based discrete-time position control of a soft continuum manipulator with proprioceptive FBG sensing. A new control algorithm has been constructed with energy-shaping principles by employing a discrete-time implementation. The stability analysis and the resulting tuning guidelines indicate that a less aggressive tuning is required in case of slower sampling or smaller physical damping. The simulations results indicate that the proposed controller achieves the prescribed regulation goal in the presence of control-related lag while preserving a consistent transient. In comparison, a baseline continuous-time controller yields a less consistent performance and would require changing the tuning parameters in different operating conditions. The experimental results clearly confirm this point. Future work will aim to extend the proposed approach to regulation in Cartesian space.

References

[1] E. Franco, A. Garriga-Casanovas, J. Tang, F. Rodriguez y Baena, and A. Astolfi, "Adaptive energy shaping control of a class of nonlinear soft continuum manipulators," *IEEE ASME Trans Mechatron*, pp. 1–11, 2021.

[2] R. L. Truby, C. D. Santina, and D. Rus, "Distributed proprioception of 3d configuration in soft, sensorized robots via deep learning," *IEEE Robotics and Automation Letters*, vol. 5, no. 2, pp. 3299–3306, apr 2020.

[3] S. Treratanakulchai and F. R. Y. Baena, "Development of a 6 DOF Soft Robotic Manipulator with Integrated Sensing Skin," in *2022 IEEE International Conference on Intelligent Robots and Systems (IROS)*. IEEE, oct 2022, pp. 1–8.

[4] K. C. Galloway, Y. Chen, E. Templeton, B. Rife, I. S. Godage, and E. J. Barth, "Fiber Optic Shape Sensing for Soft Robotics," *Soft Robotics*, vol. 6, no. 5, pp. 671–684, oct 2019.

[5] W. Zhuang, G. Sun, H. Li, X. Lou, M. Dong, and L. Zhu, "FBG based shape sensing of a silicone octopus tentacle model for soft robotics," *Optik*, vol. 165, pp. 7–15, jul 2018.

[6] A. Donder and F. R. Y. Baena, "Kalman-Filter-Based, Dynamic 3-D Shape Reconstruction for Steerable Needles With Fiber Bragg Gratings in Multicore Fibers," *IEEE Transactions on Robotics*, pp. 1–14, dec 2021.

[7] M. Stolzle and C. Della-Santina, "Piston-Driven Pneumatically-Actuated Soft Robots: modeling and backstepping control," *IEEE Control Systems Letters*, pp. 1–1, 2021.

[8] E. Franco, T. Ayatullah, A. Sugiharto, A. Garriga-Casanovas, and V. Virdyawan, "Nonlinear energy-based control of soft continuum pneumatic manipulators," *Nonlinear Dynamics*, vol. 106, no. 1, pp. 229–253, 9 2021.

[9] E. Franco, "Energy Shaping Control of Hydraulic Soft Continuum Planar Manipulators," *IEEE Control Systems Letters*, vol. 6, pp. 1748–1753, 2022.

[10] D. Laila and A. Astolfi, "Discrete-time IDA-PBC design for underactuated Hamiltonian control systems," in *2006 American Control Conference*. IEEE, 2006, p. 6 pp.

[11] S. Aoues, D. Eberard, and W. Marquis-Favre, "Discrete IDA-PBC design for 2D port-Hamiltonian systems," *IFAC Proceedings Volumes*, vol. 46, no. 23, pp. 134–139, 2013.

[12] M. Trumic, C. Della-Santina, K. Jovanovic, and A. Fagiolini, "Adaptive Control of Soft Robots Based on an Enhanced 3D Augmented Rigid Robot Matching," *IEEE Control Systems Letters*, vol. 5, no. 6, pp. 1934 – 1939, 2021.

[13] E. Franco, A. Garriga-Casanovas, and A. Donaire, "Energy shaping control with integral action for soft continuum manipulators," *Mechanism and Machine Theory*, vol. 158, pp. 1–16, apr 2021.

[14] R. Ortega, M. Spong, F. Gomez-Estern, and G. Blankenstein, "Stabilization of a class of underactuated mechanical systems via interconnection and damping assignment," *IEEE Transactions on Automatic Control*, vol. 47, no. 8, pp. 1218–1233, 8 2002.

[15] A. Garriga-Casanovas, I. Collison, and F. Rodriguez y Baena, "Toward a Common Framework for the Design of Soft Robotic Manipulators with Fluidic Actuation," *Soft Robotics*, vol. 5, no. 5, pp. 622–649, aug 2018.

[16] K. Suzumori, S. Iikura, and H. Tanaka, "Development of flexible microactuator and its applications to robotic mechanisms," in *Proceedings. 1991 IEEE International Conference on Robotics and Automation*. IEEE Comput. Soc. Press, 1991, pp. 1622–1627.

[17] I. S. Godage, R. Wirz, I. D. Walker, and R. J. Webster, "Accurate and Efficient Dynamics for Variable-Length Continuum Arms: A Center of Gravity Approach," *Soft Robotics*, vol. 2, no. 3, pp. 96–106, sep 2015.

[18] Y.-Q. Yu, L. L. Howell, C. Lusk, Y. Yue, and M.-G. He, "Dynamic Modeling of Compliant Mechanisms Based on the Pseudo-Rigid-Body Model," *Journal of Mechanical Design*, vol. 127, no. 4, p. 760, jul 2005.

[19] E. Franco, "Discrete-time IDA-PBC for underactuated mechanical systems with input-delay and matched disturbances," in *26th Mediterranean Conference on Control and Automation*. Zadar: IEEE, jun 2018, pp. 747–752.

[20] A. Astolfi, D. Karagiannis, and R. Ortega, *Nonlinear and Adaptive Control with Applications*. Berlin: Springer-Verlag, 2007.

[21] E. Franco, "Immersion and invariance adaptive control for discrete-time systems in strict-feedback form with input delay and disturbances," *International Journal of Adaptive Control and Signal Processing*, vol. 32, no. 1, pp. 69–82, sep 2018.

[22] G. Tao, "A simple alternative to the Barbălat lemma," *IEEE Transactions on Automatic Control*, vol. 42, no. 5, p. 698, 1997.

[23] D. Nesic and A. Teel, "A Framework for Stabilization of Nonlinear Sampled-Data Systems Based on Their Approximate Discrete-Time Models," *IEEE Transactions on Automatic Control*, vol. 49, no. 7, pp. 1103–1122, jul 2004.

[24] H. Khalil, *Nonlinear Systems*, 2nd ed. Upper Saddle River, NJ: Prentice-Hall, 1996.